INTERNATIONAL JOURNAL FOR NUMERICAL METHODS IN FLUIDS, VOL. 2, 1–23 (1982)

NUMERICAL CALCULATION OF TRANSITIONAL BOUNDARY LAYERS

E. ARAD, M. BERGER, M. ISRAELI AND M. WOLFSHTEIN

Technion—Israel Institute of Technology, Haifa, Israel

SUMMARY

A computational procedure for compressible axisymmetric boundary layers, on bodies of revolution, in transition from laminar to turbulent flow, is introduced. The procedure is an extension of a former method, due to Patankar and Spalding.

The flow field is computed by solution of four simultaneous equations for the momentum, the thermal energy, the turbulence energy amplitude and the turbulent scale.

The results show good agreement with existing theoretical and experimental data.

KEY WORDS Transition Boundary Layers Models of Turbulence

1. PREFACE

1.1. Introduction

This paper describes an improved method for the numerical computation of compressible axisymmetric boundary layers, around bodies of revolution, in transition from laminar to turbulent flow regime. As the heat and mass transfer coefficients between solid bodies and flowing fluids, in laminar or turbulent regimes, differ significantly from one another, the problem may be very important. For instance, in supersonic flow, where the aerodynamic heating plays an important role and may restrict the flight velocity or determine the structure and materials of the body, the flow regime has a major influence on the design. Good estimate of the transition point enables correct evaluation of the heat transfer and optimal design of the body.

The lack of basic theoretical comprehension and sufficient experimental data, imposes the use of approximate turbulence models while the complexity of the equations calls for numerical methods. In the present paper Patankar and Spalding's[1] numerical methods and Ng's turbulence model,[2] are extended to the computation of laminar, turbulent and transitional flow fields. The methods enables computation of the transition point, and the flux of momentum and energy through the solid wall, with second-order accuracy. Yet, this work does not attempt to explain the mechanism of transition from laminar to turbulent flow, and the set of constants and functions used to describe transition should be regarded as empirical information.

The present turbulence model implies that the transition phenomenon is dependent on disturbances in the potential flow, as well as the Reynolds and Mach numbers and the pressure gradient. The turbulence and the disturbance are characterized by the amplitude and the length scale. The purpose of the computation, is to find the influence of these properties on transition.

0271–2091/82/010001–23$02.30

Received September 1980
Revised 16 June 1981

1.2. Literature review

The influence of the flow regime on the heat transfer rate is known in the literature. Kays and Leung[3] computed a turbulent channel flow with a Prandtl number of 0·7. The heat transfer rate computed for turbulent flow is between 7 and 259 times larger than the heat transfer rate for laminar flow at the same Reynolds number. Comparison of laminar and turbulent heat transfer in incompressible boundary layers with a Prandtl number of 0·7 is reported by Kays,[4] who recommends for laminar flow

$$Nu_x = 0{\cdot}295\ Re_x^{0{\cdot}5}$$

and for turbulent flow

$$Nu_x = 0{\cdot}238\ Re_x^{0{\cdot}8}$$

It is obvious that for $Re_x > 4500$ the Nusselt number in turbulent flow is significantly higher than in laminar flows. Similar results for a compressible boundary layer were obtained by van Driest[5] and Deissler and Loeffler.[6]

Despite the importance of the subject, the prediction of the transition point is still difficult, and an adequate theory is still lacking. Furthermore, experimental results are inconsistent within themselves, and the characteristics of transition-causing disturbances is not reported in many experiments. This situation is reviewed by Reshotko[7] and Morkovin.[8,9]

A surprising aspect of the existing experimental data is the possibility of getting good correlations within distinct groups of experiments, when the flow is characterized by the dimensional 'Unit Reynolds Number' defined as

$$\frac{\rho U}{\mu}$$

This indicates the existence of a length scale (typical to the experimental apparatus perhaps), by which a disturbance Reynolds number might be defined. Some such scales were proposed in the literature: Reshotko[10] related the length scale to the length corresponding to the slowest disturbance waves, as calculated from the linear stability theory. Emmons[11] and Nagel[12] related the length to the distance between the 'heads' of Tollmien–Schlichting waves where sudden local bursts of turbulence appear. Another assumption was that the distance between wave 'heads' depends on the intensity of turbulence in the potential flow. Pate[13] had a different approach: He assumed, following Laufer,[14] that the acoustic waves transmitted from the walls of supersonic wind tunnels are the major sources of transition-causing disturbances. The correlation suggested in his paper was between the transition Reynolds number and the thickness of the acoustic wave-generating boundary layer.

In the light of this discussion, it seems that the transition location is determined by the characteristics of the disturbances outside the boundary layer. Consequently, transport of the amplitude and the length scale of fluctuations from the main flow should be computed. Such computation should be based on solution of adequate differential equations, e.g. for the turbulent energy and for the length scale. This approach is difficult in reality, as it requires a good turbulence model as well as computational methods. As a result, the researchers generally use simplified approaches, attempting to characterize disturbances by one parameter only, or by empirical correlations. Thus, Harris[15] computed the transition point by empirical formulae, while Reshotko,[10] Nagel[12] and Pate[13] characterized the transition location by the length scale of the disturbances only.

A different approach was developed by Shamroth and McDonald[16] and McDonald and Fish[17] who related the disturbances to the amplitude of the fluctuations, and computed its

diffusion into the boundary layer by solution of the turbulent energy equation. Donaldson[18] used a similar approach, solving for the Reynolds stresses in the boundary layer, in the transition area.

The common disadvantage of all these works lies in the fact that none of them tried to compute the diffusion of both the turbulent energy and length scale into the boundary layer. In the present research, an attempt was made to perform such a computation. Success of this approach depends on the development of a low turbulence two-equation model, to be coupled with one of the available models for turbulent boundary layer calculations.

Ng,[2] Wolfshtein,[19] and Rotta[20] solved the equations for the turbulent energy and scale. Jones and Launder[21] and Harlow and Nakayama[22] replaced the scale equation by an equation for the dissipation of turbulent energy into thermal energy, while Glushko[23] solved an equation for the square of the scale, and Saffman[24] and Wilcox and Alber,[25] solved an equation for the fluctuation vorticity. Wolfshtein *et al.*[26] showed that all these models have a similar general form, differing mainly in some empirical coefficients. Nonetheless, their models differ from one another in the low turbulence approximation, required in the viscous sublayer near the wall, and in the numerical techniques used to obtain a solution.

For the present work, a model that contains Ng's turbulence scale equation[2] was chosen, mainly because this model is well documented, and shows favourable agreement with a large number of turbulent boundary layer experimental data.

1.3. The present work

Computation of the flow field in transition from laminar to turbulent regime, is performed in this work by solving the equations for turbulent energy and its scale, together with equations for the momentum and thermal energy. The turbulence model is based on Ng's work[2] with Wolfshtein's modifications.[19]

A modified Patankar and Spalding[1] numerical method is used. The present method is of second order. In order to account for strong gradients near the wall (particularly in turbulent flow), transformations of the lateral co-ordinates are applied, so as to condense the grid points near the wall. Thus, the wall functions used in Reference 1 are removed.[27]

The present method was successfully tested for laminar, turbulent and transitional flows, for compressible and incompressible cases, on a flat plate, without pressure gradient, and on bodies of revolution. The numerical properties of this method were discussed by Berger *et al.*[27]

2. MATHEMATICAL FORMULATION

2.1. The co-ordinate system

A curvilinear orthogonal co-ordinate system is convenient for boundary layer calculations near the surface of bodies of revolution. In such systems the x-axis is parallel to the body surface, while the y-axis is normal to the body. An illustration of the system is presented in Figure 1. The flow region of interest lies between the internal wall, designated by the subscripts 'w' and the external boundary designated by '∞', or by 'E'. Two parameters define the body curvature:

(i) r—the distance between the axis of symmetry and the point under consideration.

(ii) α—the angle between the tangent to the surface $y = \text{const.}$ and the axis of symmetry.

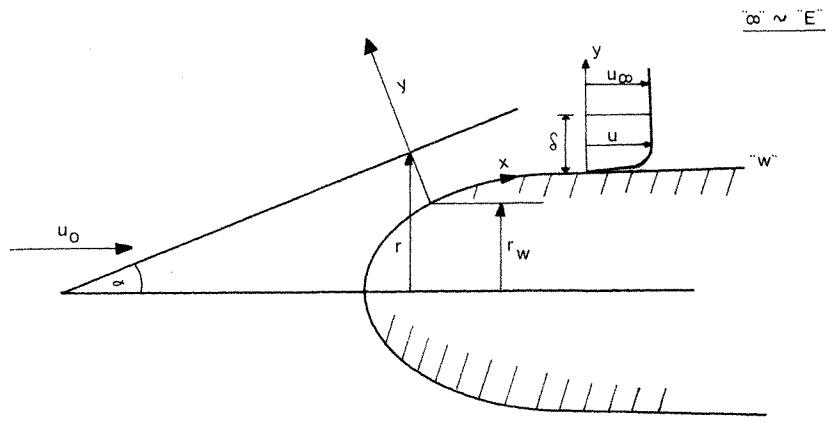

Figure 1. Co-ordinate system

Obviously, the radius in a particular point is given by:

$$r = r_w + \left[\int_0^y \cos\alpha(\eta)\,d\eta\right]_{x=\text{const.}} \tag{1}$$

When the thickness of the boundary layer, δ, is small relative to the radius of the body

$$\frac{\delta}{r_w} \ll 1$$

equation (1), degenerates to:

$$r = r_w = r(x)$$

(This simplification is not used in subsection 2.2.)

The present work is limited to cases in which the angle of attack, between the main flow and the axis of the body, is zero. In this case the flow is axisymmetric, and the equations are two-dimensional, in the sense that there are only two independent variables (x, y), as defined above.

2.2. *The governing equations*

2.2.1. *The conservation equations.* The conservation equations for mass, momentum and energy, for a steady boundary layer, are

$$\frac{\partial}{\partial x}(\rho u r) + \frac{\partial}{\partial y}(\rho v r) = 0 \tag{2a}$$

$$\rho u\frac{\partial u}{\partial x} + \rho v\frac{\partial u}{\partial y} = -\frac{\partial p}{\partial x} + \frac{1}{r}\frac{\partial}{\partial y}\left(\mu_{\text{eff}}\, r\frac{\partial u}{\partial y}\right) \tag{2b}$$

$$\rho u\frac{\partial h_0}{\partial x} + \rho v\frac{\partial h_0}{\partial y} = \frac{1}{r}\frac{\partial}{\partial y}\left\{r\left[\frac{\mu_{\text{eff}}}{\sigma_h}\frac{\partial h_0}{\partial y} + \left(1-\frac{1}{\sigma_h}\right)\mu_{\text{eff}}\frac{\partial}{\partial y}\left(\frac{u^2}{2}\right)\right]\right\} \tag{2c}$$

The unknowns in these equations are the velocity components u and v, and the stagnation ethalpy h_0. Equations (2b) and (2c) are parabolic partial differential equations.

2.2.2. *The initial and boundary conditions.* The momentum and energy equations need the usual boundary conditions. The velocity is zero on the wall. Outside the boundary layer the velocity is equal to the specified potential velocity, u_∞.

The enthalpy outside of the boundary layer is determined by the solution of the external flow, which is usually an isentropic solution. Other boundary conditions can be applied as well. On the wall two boundary conditions for energy are possible: Either a given heat flux or a given temperature. In the present work an adiabatic wall is assumed, with $(\partial T/\partial y)_w = 0$.

For the solution of parabolic equations, initial profiles of the variables are required. These initial profiles can be obtained from experimental data, empirical relations, approximate theories or guesswork. In this work the Karman–Pohlhausen velocity profile and the Crocco temperature–velocity relation are used. Details of these profiles are given below. The initial boundary layer thickness δ_0 should be specified as well.

2.2.3. *The thermodynamic relations.* The presure p, is usually determined by the external flow conditions. Other thermodynamic properties are computed by the following auxiliary relations:

$$T = \frac{h_0 - \frac{u^2}{2}}{C_p} \tag{3}$$

$$\rho = \frac{pW}{RT} \tag{4}$$

$$\mu = \mu_R \left[\frac{T}{T_R}\right]^{3/2} \left[\frac{T_R + T_v}{T + T_v}\right] \tag{5}$$

where μ_r is the air viscosity at temperature T_R and

$$T_v = 110°\text{K}$$

$$W = 28{\cdot}8 \text{ kgm/kg mole}$$

$$C_p = \gamma R/[(\gamma - 1)W] \tag{6}$$

The universal gas constant is $R = 8{\cdot}317$ J/mole°K and the specific heat ratio is $\gamma = 1{\cdot}4$.

The effective viscosity is the sum of the laminar and the turbulent viscosities:

$$\mu_{\text{eff}} = \mu + \mu_t \tag{7}$$

The calculation method of μ_t is described in the next section.

2.3. *The turbulence model*

2.3.1. *The governing equations.* The turbulence model that is used in this work was proposed by Ng.[2] In this model, the turbulence is defined by the turbulent energy e and its scale l, which are defined as follows:

$$e = \tfrac{1}{2}(\overline{u'^2} + \overline{v'^2} + \overline{w'^2}) = \int_0^\infty E(k)\,\mathrm{d}k$$

$$l = \frac{1}{e}\int_0^\infty \frac{E(k)}{k}\,\mathrm{d}k$$

where k is the wave number and $E(k)$ is the one-dimensional spectral distribution of the energy.

The governing equations for e and l are:

$$\rho\frac{De}{Dt}=\frac{\partial}{\partial y}\left[\left(\mu+\frac{\mu_t}{\sigma_e}\right)\frac{\partial e}{\partial y}\right]+\mu_t\left(\frac{\partial u}{\partial y}\right)^2-\frac{C_1}{f_1}\rho\frac{e^{3/2}}{l} \tag{8a}$$

$$\rho\frac{D(el)}{Dt}=\frac{\partial}{\partial y}\left[\left(\mu+\frac{\mu_t}{\sigma_l}\right)\frac{\partial(el)}{\partial y}\right]\left(C_2f_2-\frac{F_4}{f_4}\right)l\mu_t\left(\frac{\partial u}{\partial y}\right)^2-\frac{C_3}{f_3}\rho e^{3/2} \tag{8b}$$

The turbulent viscosity is given by:

$$\mu_t=C_\mu f_\mu\rho e^{1/2}l \tag{9}$$

and F_4 is defined as:

$$F_4=\left(C_4\frac{l}{y}\right)^q \tag{10}$$

The constants C_μ, C_1, C_2, C_3, C_4, σ_e, σ_l, q, were chosen by Ng in order to get good agreement between the theory and a large number of turbulent boundary layer flows for which reliable experimental data is available. For a low turbulence level the functions, f_μ, f_1, f_2, f_3, f_4 were added following Wolfshtein.[19] These functions approach unity at a high turbulence level. The turbulence level is estimated by the turbulent Reynolds number:

$$\mathrm{Re}_t=\frac{\rho e^{1/2}l}{\mu} \tag{11}$$

The functional form of f_μ, f_1, f_2, f_3, f_4 is as follows:

$$f_\mu=1-\exp(-A_\mu\mathrm{Re}_t) \tag{12a}$$

$$f_1=1-\exp(-A_1\mathrm{Re}_t) \tag{12b}$$

$$f_2=1-\exp(-A_2y_+) \tag{12c}$$

$$f_3=1-\exp(-A_3\mathrm{Re}_t) \tag{12d}$$

$$f_4=[1-\exp(-A_4l_+)]^t \tag{12e}$$

$$l_+=\frac{l\sqrt{(\tau_w\rho)}}{\mu} \tag{13}$$

$$y_+=\frac{y\sqrt{(\tau_w\rho)}}{\mu} \tag{14}$$

The empirical constants A_μ, A_1, A_2, A_3, A_4, t are chosen to obtain the best agreement with experimental data. The values are summarized in Table I, together with the other constants, which are identical to Ng's recommendations.

Table I

$C_1=0{\cdot}09$	$A_1=0{\cdot}892$	$\sigma_e=1$
$C_2=0{\cdot}98$	$A_2=0{\cdot}038$	$\sigma_l=1$
$C_3=0{\cdot}058$		$q=6$
	$A_4=0{\cdot}855$	$t=4$
$C_\mu=1$	$A_\mu=0{\cdot}127$	$K=0{\cdot}41$

$C_4=[(KC_1^{1/4}+C_1C_2-C_3)/C_1]^{1/6}/KC_1^{1/4}$

$A_3=(5{\cdot}2169-1{\cdot}9602/A_4^4)^{-1}$

2.3.2. *Initial and boundary conditions, and auxiliary relations.* On the wall, both e and el are set at zero. On the external boundary they reach the main flow values. Sometimes a prescription of uniform values for e and l is sufficient. However, a better estimate is obtained by the solution of the homogeneous flow form of equations (8a) and (8b), namely

$$\frac{\partial e_\infty}{\partial x} = C_1 \frac{e_\infty^{3/2}}{U_\infty l_\infty} \tag{15a}$$

$$\frac{\partial l_\infty}{\partial x} = (C_1 - C_3) \frac{e_\infty^{1/2}}{U_\infty} \tag{15b}$$

The initial profiles for e and el are discussed below. The effective Prandtl number σ_{eff} is given by

$$\frac{1}{\sigma_{\text{eff}}} = \frac{\dfrac{\mu}{\sigma} + \dfrac{\mu_t}{\sigma_t}}{\mu + \mu_t} \tag{16}$$

where σ, σ_t are the effective laminar and turbulent Prandtl numbers respectively.

2.4. *Transformations and final formulations*

2.4.1. *General equation.* The equations of momentum (2b), thermal energy (2c), turbulent energy (8a) and length scale (8b), have a similar form. This can be utilized in order to obtain a single procedure for their solution. First, we write an equation for a general variable ϕ:

$$\rho u \frac{\partial \phi}{\partial x} + \rho v \frac{\partial \phi}{\partial y} = \frac{1}{r} \frac{\partial}{\partial y} \left[\Gamma r \frac{\partial \phi}{\partial y} \right] + s \tag{17}$$

where ϕ, Γ and s are given in the following table:

Table II

Equation no.	ϕ	Γ	s
(2b)	u	μ_{eff}	$-\dfrac{dp}{dx}$
(2c)	h_0	$\dfrac{\mu_{\text{eff}}}{\sigma_{h_{\text{eff}}}}$	$\dfrac{\partial}{\partial y}\left[\left(1 - \dfrac{1}{\sigma_{h_{\text{eff}}}}\right)\mu_{\text{eff}} \dfrac{\partial}{\partial y}\left(\dfrac{u^2}{2}\right)\right]$
(8a)	e	$\mu + \dfrac{\mu_t}{\sigma_{e_t}}$	$\mu_t \left(\dfrac{\partial u}{\partial y}\right)^2 - \dfrac{C_1}{f_1} \rho \dfrac{e^{3/2}}{l}$
(8b)	el	$\mu + \dfrac{\mu_t}{\sigma_{el_t}}$	$\left(C_2 f_2 - \dfrac{F_4}{f_4}\right)\mu_t \left(\dfrac{\partial u}{\partial y}\right)^2 - \dfrac{C_3}{f_3} \rho e^{3/2}$

The effective Prandtl number is given by equation (16) above.

2.4.2. *Co-ordinate transformations.* The (x, y) co-ordinates system is not very convenient for numerical calculations. An ideal co-ordinate system would cover the important parts of the flow field, with stretching in special regions. In particular the following properties appear very desirable:

(i) The cross-stream co-ordinate should vary between zero and unity.

(ii) The continuity equation should be uncoupled from the momentum equation.

(iii) The cross-stream co-ordinate should be linear and dense in the region of steep gradients near the wall.

(iv) The final equation should be as simple as possible.

A co-ordinate system which satisfies these requirements is obtained through the following stages:

2.4.2.1 Patankar–Spalding transformation

A transformation from (x, y) to (x, ω) was suggested by Patankar and Spalding.[1] The transformation is defined as follows:

$$\omega = \frac{\psi}{\psi_E} \tag{18}$$

where

$$\psi = \left[\int_0^Y \rho u r \, dy\right]_{x=\text{const.}} \tag{19}$$

or in the usual way

$$\rho u r = \frac{\partial \psi}{\partial y} \tag{20a}$$

$$-\rho v r = \frac{\partial \psi}{\partial x} \tag{20b}$$

and ψ_E is the value of the stream function at the edge of the boundary layer. In this co-ordinate system, the continuity equation is satisfied automatically because of the use of stream function co-ordinates.

The general equation (17) transforms to the form:

$$\frac{\partial \phi}{\partial x} + b\omega \frac{\partial \phi}{\partial \omega} = \frac{\partial}{\partial \omega}\left(\frac{c}{\sigma}\frac{\partial \phi}{\partial \omega}\right) + d \tag{21}$$

where

$$b = \frac{r_E \dot{m}''_E}{\psi_E} \tag{21a}$$

$$c = \frac{r^2 \rho \Gamma}{\psi_E^2} \tag{21b}$$

$$d = \frac{s}{\rho u} \tag{21c}$$

For the velocity:

$$\sigma = 1 \tag{22a}$$

$$d = -\frac{1}{\rho u}\frac{dp}{dx} \tag{22b}$$

For the stagnation enthalpy:

$$\sigma = \sigma_h \tag{23a}$$

$$d = \frac{\partial}{\partial \omega}\left[\mu_{\text{eff}}\left(1 - \frac{1}{\sigma_h}\right)\frac{\rho u r^2}{\psi_E^2}\frac{\partial}{\partial \omega}\left(\frac{u^2}{2}\right)\right] \tag{23b}$$

The (x, ω) co-ordinates are similar to the von Mises co-ordinates, but while the von Mises cross-stream co-ordinate, ψ, can vary without limit, ω is bounded between zero and unity.

The form of the equation is slightly more complicated than the von Mises equation, having an additional term in the left-hand side of the equation.

One important property of the von Mises co-ordinates, namely the automatic guarantee of continuity is kept here as well. Thus, the normal velocity, v, is not needed during computation. Moreover, the grid is absolutely self-adaptive to the thickness of the boundary layer.

2.4.2.2. Elimination of the wall singularity

The transformation to (x, ω) was revealed to be unsuccessful near the solid wall for laminar incompressible flow[27] where the velocity is given by

$$u = cy \tag{24}$$

substitution of (24) in (18) and (19) gives

$$\omega = \frac{c}{2\psi_E} y^2 \tag{25a}$$

$$y = \left(\frac{2\psi_E \omega}{c}\right)^{0.5} \tag{25b}$$

$$u = (2c\psi_E \omega)^{0.5} \tag{25c}$$

Consequently a Taylor series expansion (which is the basis for finite difference approximation) of u in ω, does not exist near the wall. The normal derivative of the velocity near the wall, with respect to ω, becomes

$$\frac{\partial u}{\partial \omega} = \left(\frac{c\psi_E}{2\omega}\right)^{0.5} \tag{25d}$$

Therefore

$$\lim_{\omega \to 0} \left(\frac{\partial u}{\partial \omega}\right) = \infty$$

This uncontrolled growth causes gross inaccuracy in the computation near the wall. Moreover, the finer the mesh the larger the error associated with this singularity. Berger *et al.*[27] resolved the problem by the following transformation:

$$\omega = z^2 \tag{26}$$

Now, near the solid wall ($y = \omega = z = 0$)

$$u = (2c\psi_E \omega)^{0.5} = (2c\psi_E)^{0.5} z \tag{27a}$$

$$\frac{\partial u}{\partial y} = (2c\psi_E)^{0.5} \tag{27b}$$

and the problem is solved.

Under this transformation the general equation (21) has the following form:

$$\frac{\partial \phi}{\partial x} + \frac{b}{2} z \frac{\partial \phi}{\partial z} = \frac{1}{2z} \frac{\partial}{\partial z} \left(\frac{c}{2z\sigma} \frac{\partial \phi}{\partial z}\right) + d \tag{28}$$

2.4.2.3. Co-ordinate stretching

The transformation from (x, ω) to (x, z) co-ordinates, gives good solution for the laminar case. The scaling of the stream function between zero and unity, which is invariant through

the transformation to (x, z), enables the use of a finite differences grid which covers all the boundary layer, without 'wasting' points on the potential area.

Unfortunately, the self-adaptive grid created in this way is inefficient for the turbulent flow calculations. In this flow, strong velocity gradients occur in the viscous sub-layer, in the vicinity of the solid wall. This layer is very thin in comparison to the whole layer, and uniform distribution of the grid points in z causes the second mesh point to move out of that sub-layer. Patankar and Spalding[1] solved this problem by the use of wall functions and fictitious points near the wall. However, this practice resulted in the loss of the second-order accuracy. Another possibility is to enlarge the number of grid points. Yet, this would have made the computer time demands very severe, and would have reduced the efficiency of the program. (Two thousand grid points in the lateral direction were found to be still insufficient for good accuracy in the viscous sublayer.)

As a result of this difficulty, a variable grid with a small mesh size in the vicinity of the solid wall is required. Indeed, the transformation to (x, z) causes a certain condensation of the mesh near the wall, but this is not sufficient, and the following transformation to (x, ζ) is proposed.

$$\begin{aligned} \zeta &= A \operatorname{tg}^{-1}(z/\beta) \\ 1/\beta &= \operatorname{tg}^{-1}(1/A) \end{aligned} \tag{29}$$

where A is a constant chosen for numerical efficiency, and is discussed in subsection 3.3 below. The transformed co-ordinate, ζ, varies between zero and unity. On the wall

$$y = \omega = z = \zeta = 0 \tag{30a}$$

and on the potential flow boundary

$$w = z = \zeta = 1 \tag{30b}$$

so that

$$z = \frac{\operatorname{tg}\left(\frac{\zeta}{A}\right)}{\operatorname{tg}\left(\frac{1}{A}\right)} \tag{31a}$$

Near the wall the velocity is linear in z, and for $z \to 0$

$$[u]_{\zeta \to 0} = \frac{(2c\psi_E)^{0.5}}{A \operatorname{tg}\left(\frac{1}{A}\right)} \cdot \zeta \tag{31b}$$

Thus the singularity problem does not arise in the computation.

Under this transformation the general equation is:

$$\frac{\partial \phi}{\partial x} + b\tilde{\Lambda}\frac{\partial \phi}{\partial \zeta} = \Lambda \frac{\partial}{\partial \zeta}\left(\frac{c}{\sigma}\Lambda \frac{\partial \phi}{\partial \zeta}\right) + d \tag{32}$$

where

$$\Lambda = \frac{1}{2z}\frac{\partial \zeta}{\partial z} = \frac{A \operatorname{tg}^2\left(\frac{1}{A}\right)\cos^2\left(\frac{\zeta}{A}\right)}{2 \operatorname{tg}\left(\frac{\zeta}{A}\right)} \tag{32a}$$

$$\tilde{\Lambda} = z^2\Lambda = \frac{A}{4}\sin\left(2\frac{\zeta}{A}\right) \tag{32b}$$

The singularity of Λ near the wall ($\zeta = 0$) causes extreme stiffness of equation (32). This dictates the use of special implicit schemes, as discussed by Berger *et al.*,[27] to avoid oscillations. The simplest such scheme is the first-order fully implicit scheme described below. The source terms are given by:

$$d_u = -\frac{1}{\rho u}\frac{dp}{dx} \tag{33a}$$

$$d_{h_0} = \Lambda \frac{\partial}{\partial \zeta}\left[\mu_{\text{eff}}\left(1-\frac{1}{\sigma_h}\right)\frac{r^2}{\psi_E^2}\Lambda \frac{\partial}{\partial \zeta}\left(\frac{u^2}{2}\right)\right] \tag{33b}$$

$$d_e = \mu_t \frac{\rho u r^2}{\psi_E^2}\Lambda^2\left(\frac{\partial u}{\partial \zeta}\right)^2 - \frac{C_1}{f_1}\rho\frac{e^{3/2}}{l} \tag{33c}$$

$$d_{el} = \left(C_2 f_2 - \frac{F_4}{f_4}\right) l\mu_t \frac{\rho u r^2}{\psi_E^2}\Lambda^2\left(\frac{\partial u}{\partial \zeta}\right)^2 - \frac{C_3}{f_3}\rho e^{3/2} \tag{33d}$$

The initial profiles are prescribed in terms of the transformed normal co-ordinates, z or ζ. Two possibilities arise: for laminar or transitional boundary layers, laminar initial profiles are prescribed. For turbulent boundary layers, turbulent initial profiles are required. The initial laminar velocity profile is approximated by the Karman–Pohlhausen profile:

$$\frac{u}{u_\infty} = F(z) + \lambda G(z) \tag{34}$$

$$F(z) = 2z - 2z^3 + z^4 \tag{34a}$$

$$\lambda = -\frac{dp}{dx}\frac{1}{\rho_\infty U_\infty} \tag{34b}$$

$$G(z) = \tfrac{1}{6}(z - 3z^2 + 3z^3 - z^4) \tag{34c}$$

where z varies between zero on the wall and unity on the potential flow boundary. For adiabatic wall the temperature is related to the velocity by the Crocco integral:

$$\frac{T}{T_\infty} = 1 - r_f\frac{(\gamma-1)}{2}M^2\left(1-\frac{u^2}{u_\infty^2}\right) \tag{35}$$

where r_f is the recovery factor and the enthalpy is given by

$$h_0 = c_p T + \left(\frac{u^2}{2}\right) \tag{36}$$

The turbulent properties are:

$$L = \left(\frac{L_\infty}{\delta}\right)z \tag{37}$$

$$\frac{e}{u_\infty^2} = c_e^2 z^2 \tag{38}$$

The parabolic turbulence energy distribution represents a very low level of turbulence, and a low turbulent viscosity, as expected when the flow is laminar.

For fully turbulent flows initial turbulent profiles are required. The turbulent velocity profile is based on the seventh power low velocity profile

$$\frac{u}{u} = \eta^{1/7} \tag{39}$$

$$\eta = \frac{y}{\delta} = [z(\zeta)]^{1.75} \tag{39a}$$

In this case the initial turbulence energy may be approximated by

$$e = \begin{cases} e_M \left(\dfrac{\eta}{\eta_M}\right)^2 & \eta \le \eta_M \\ e_E + \left(\dfrac{e_M - e_E}{2}\right)\left[\dfrac{(1-\eta)}{(1-\eta_M)} + \left(\dfrac{1-\eta}{1-\eta_M}\right)^2\right] & \eta > \eta_M \end{cases} \tag{40}$$

where

$$\eta_M = \frac{12}{\delta}\left(\frac{\mu}{\rho\left(\dfrac{\partial u}{\partial y}\right)_w}\right)^{0.5} \tag{40a}$$

$$e_M = 3{\cdot}15u_\infty^2\left[\left(1+0{\cdot}88\left(\frac{\gamma-1}{2}\right)\right]u^2 c_p\right. \tag{40b}$$

$$e_E = c_k^2 u_\infty^2 = (u')^2 \tag{40c}$$

The length scale profile is

$$l = \begin{cases} Kc_1^{1/4} y & 0 \le y < \dfrac{\lambda}{K}\delta \\ \lambda c_1^{1/4}\delta & \dfrac{\lambda}{K}\delta \le y < \delta \end{cases} \tag{41}$$

The temperature and stagnation enthalpy are given by equations (35) and (36) as in the laminar case.

3. THE NUMERICAL METHOD

3.1. General description

The set of simultaneous equations with suitable boundary conditions and auxiliary relations, is solved numerically. This is done by solving the equations one after the other, using the same procedure. For this reason, it suffices to discuss here the solution of the general equation (32). This equation is parabolic and non-linear. Patankar and Spalding[1] solved such equations using an implicit method, and wall functions and fictitious points to account for the region adjacent to the wall. Their method, which was used in the first stage of the present work, is of first-order accuracy at most. In the present research second-order central differences are used in the normal direction, and wall functions are not applied.

For the streamwise direction a forward derivative is chosen, so the accuracy in this direction is of first order. This accuracy is sufficient because in boundary layer problems, the variation in the mainstream direction is much slower than the variation in the normal

direction. The finite difference equation for the general equation, is obtained by integration over small control volumes, around the grid points. The resulting equation is:

$$\left[\frac{\left(\frac{c\Lambda}{\sigma}\right)_{i+1/2,u}}{h^2}-\frac{b_{i,U}z_i^2}{2h}\right]\phi_{i+1,D}+\left[\frac{\left(\frac{c\Lambda}{\sigma}\right)_{i-1/2,U}}{h^2}+\frac{b_{i,U}z_i^2}{2h}\right]\phi_{i-1,D}$$

$$=\left[\frac{\left(\frac{c\Lambda}{\sigma}\right)_{i+1/2,U}+\left(\frac{c\Lambda}{\sigma}\right)_{i-1/2,U}}{h^2}+\frac{1}{k\Lambda_i}-\frac{s_{i,D}}{\Lambda_i}\right]\phi_{i,D}=\frac{\phi_{i,U}}{k\Lambda_i}-\frac{s_{i,U}}{\Lambda_i} \quad (42)$$

where h and k are the grid sizes in the ζ and x directions. The source term is split into two parts

$$d_i = s_{i,U} + s_{i,D}\phi_{i,D} \quad (43)$$

where $s_{i,U}$ and $s_{i,D}$ are computed upstream. For numerical reasons, it is preferable to make $s_{i,U}$ as small as possible.

Equation (42) has the general form

$$\phi_i = A_i\phi_{i+1} + B_i\phi_{i-1} + C_i \quad (44)$$

It is apparently implicit, but the implicitness is only partially complete, for A_i, B_i, C_i are usually functions of ϕ, while the solution method assumes they are given coefficients (computed according to the upstream ϕ values). Thus it is necessary to use small integration steps in order to obtain good accuracy, although stability is independent of the step size because of the implicitness of the method.

The coefficient matrix of equation (42) is three-diagonal, and is solved using the Thomas algorithm. Equation (42) can be written in the form:

$$\alpha_{i,U}\phi_{i+1,D} + \beta_{i,U}\phi_{i-1,D} = \gamma_{i,U}\phi_{i,D} + \delta_{i,v} \quad (45)$$

The condition for stability is

$$\left.\begin{aligned}\alpha_{i,U} &> 0\\ \beta_{i,U} &> 0\end{aligned}\right\} \quad (46)$$

This condition is always satisfied for the finite difference form of equation (42). However, when injection (or suction) is applied, equation (42) should be modified, and condition (46) is not satisfied. In such cases it is necessary to use upwind first-order finite differences to ensure stability.

3.2. *Treatment of source term*

The source term has two components: one is calculated at the upstream integration step, while the other is a linear function of the present value of ϕ. Stability and accuracy are usually improved when $S_{i,U}$ is minimized. The source terms, as defined in equations (17) and (21c) are given below.

For the momentum equation

$$\left.\begin{aligned}s_{i,U} &= d_{i,U} = -\left(\frac{1}{\rho u}\frac{dp}{dx}\right)_i\\ s_{i,D} &= 0\end{aligned}\right\} \quad (47)$$

For the stagnation enthalpy,

$$s_{h_0,i,U} = d_{h_0,i} = \left\{\frac{1}{\rho u}\frac{\partial}{\partial y}\left[\left(1-\frac{1}{\sigma_{\text{eff}}}\right)\mu_{\text{eff}}\frac{\partial}{\partial y}\left(\frac{u^2}{2}\right)\right]\right\}_i \qquad (48)$$

$$s_{h_0,i,D} = 0$$

The equations for the turbulent energy and the scale require more careful treatment. Here splitting of the source terms is somewhat complex due to the non-linearity of the sources. Yet careful examination reveals that the dissipation may be separated from the generation, to give, for the turbulent energy:

$$\left.\begin{aligned} s_{e,i,U} &= \left[\mu_t\left(\frac{\partial u}{\partial y}\right)^2 \Big/ \rho u\right]_{i,U} \\ s_{e,i,D} &= \left[-\frac{1}{u}\frac{C_1}{f_1}\left(\frac{e^{1/2}}{l}\right)\right]_{i,U} \end{aligned}\right\} \qquad (49)$$

and for the turbulent scale:

$$\left.\begin{aligned} s_{el,i,U} &= \left[\left(C_2 f_2 - \frac{F_4}{f_4}\right) l\mu_t\left(\frac{\partial u}{\partial y}\right)^2\right] \Big/ \rho u\Big\}_{i,U} \\ s_{el,i,D} &= \left[-\frac{1}{4}\frac{C_3}{f_3}\left(\frac{e^{1/2}}{l}\right)\right]_{i,U} \end{aligned}\right\} \qquad (50)$$

In order to prevent numerical instability of the length scale equation near the solid wall, as a result of the quick growth of F_4, which contains a sixth power of (l/y), the following limitation was set on F_4

$$\left(C_2 f_2 - \frac{F_4}{f_4}\right) > 0 \qquad (51)$$

This limitation is met by application of the following condition near the solid wall

$$l \leq K C_1^{1/4} y \qquad (52)$$

which is the solution of the length scale equation for a one-dimensional logarithmic boundary layer.

3.3. Mesh stretching and grid size

As mentioned above a stretching transformation (29) was necessary to ensure sufficient accuracy near the wall. The transformation was chosen so as to satisfy the following requirements:

(a) At least half the grid points should be in the first per cent of the boundary layer width.

(b) A reasonable number of points should be near the potential flow boundary.

Following these requirements the β coefficient of the transformation was chosen

$$\beta = 0{\cdot}001$$

The number of the grid points is chosen so as to give a good description of the viscous sub-layer. In order to find the necessary number of points, incompressible flow on a flat plate without pressure gradient was studied. The number of points varied between 30 and 200. The resulting transition Reynolds numbers, based on the displacement thickness, are presented in Figure 2. It appears, that for 120–150 grid points, variation of the number of

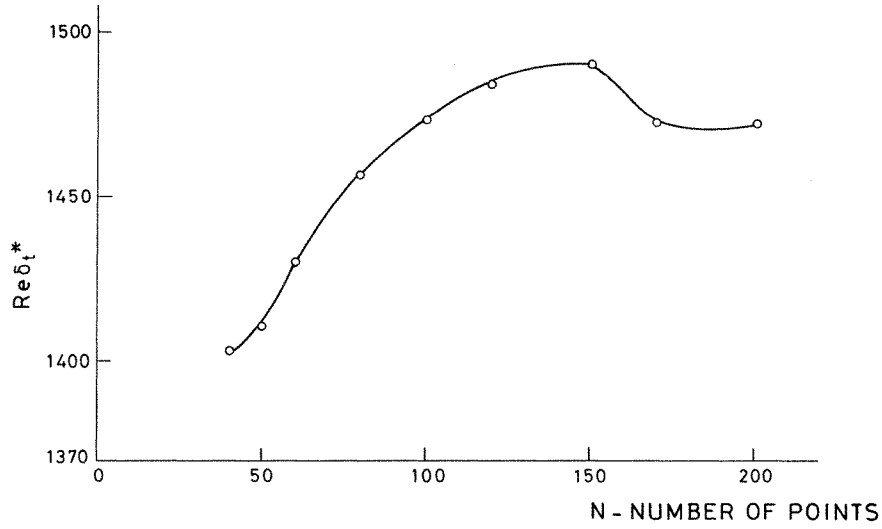

Figure 2. The effect of the number of mesh points on the Reynolds number of transition from laminar to turbulent flow, on a flat plate, without pressure gradient

mesh points caused a small difference, but for $N>150$, oscillations of the solution appear, apparently by the computer round-off error. Therfore, a 150-point grid was chosen, in order to get the optimal accuracy. This number is not too large, and the price of the computations is not prohibitive.

The integration step in the x-direction is limited by the following conditions:

$$\Delta x \leq \delta/2 \tag{53a}$$

$$\Delta x \leq \frac{\psi_E}{100 r_E \dot{m}''_E} \tag{53b}$$

Both conditions may be justified on physical grounds. Their aim is to limit the boundary layer growth per step, either by comparing the grid size to the boundary layer thickness or by comparing the entrainment per step to the total mass flow in the boundary layer.

3.4. The skin friction

The friction coefficient on the wall is defined as

$$c_f = \frac{\tau_w}{\frac{1}{2}\rho_\infty u_\infty^2} \tag{54}$$

with

$$\tau_w = \mu\left(\frac{\partial u}{\partial y}\right)_{y=0} = \mu\left(\frac{\partial u}{\partial \zeta}\ \frac{\partial \zeta}{\partial z}\ \frac{\partial z}{\partial \omega}\ \frac{\partial \omega}{\partial y}\right)_{y=0} \tag{55}$$

These four derivatives are calculated in the following way:

(i) The derivative of the velocity near the wall is calculated to second order by a one-sided formula. Denoting the finite difference mesh point on the wall as point number 1, and

recalling that $u_1 = 0$, we may write

$$\left(\frac{\partial u}{\partial \zeta}\right)_1 = \frac{4u_2 - u_3}{2\Delta\zeta} + O(\Delta\zeta^2) \tag{56}$$

(ii) The second derivative in equation (55) is obtained from equation (29) as

$$\frac{d\zeta}{dz} = \frac{A \operatorname{tg}(1/A)}{1 + z^2 \operatorname{tg}^2(1/A)} \tag{57}$$

(iii) The third derivative is singular near the wall:

$$\lim_{z\to 0} \frac{dz}{dw} = \lim_{z\to 0} \frac{1}{2z}$$

Therefore we have to calculate:

$$\frac{dz}{d\omega}\frac{\partial \omega}{\partial y} = \frac{dz}{dy} = \frac{1}{2z}\frac{\rho u r}{\psi_E} = \frac{\rho r}{2\psi_E}\frac{u}{z} \tag{58}$$

but near the wall u is linear in y or z to second order and therefore

$$\lim_{z\to 0}\left(\frac{u}{z}\right) = \lim_{z\to 0}\left(\frac{\partial u}{\partial z}\right)$$

Therefore

$$\tau_w = \mu_w \frac{\rho r}{2\psi_E}\left(\frac{\partial u}{\partial \zeta}\right)^2\left(\frac{\partial \zeta}{\partial z}\right)^2 \tag{59}$$

3.5. Calculation of the normal distance, y

The normal co-ordinate y and its derivative depend on ρ, u, r, ζ. The derivative is computed according to the chain rule using (18), (20à), (26) and (29):

$$\frac{\partial y}{\partial \zeta} = \frac{\partial y/\partial \zeta}{\partial z/\partial z} = \frac{2\psi_E z(\beta + z)}{\rho u r A} \tag{60}$$

The following fourth-order integration algorithm is used to calculate y:

$$y_i = y_{i-2} + 2h\left[\frac{1}{6}\left(\frac{\partial y}{\partial \zeta}\right)_i + \frac{2}{3}\left(\frac{\partial y}{\partial \zeta}\right)_{i-1} + \frac{1}{6}\left(\frac{\partial y}{\partial \zeta}\right)_{i-2}\right] + O(h^4) \tag{61}$$

3.6. Scope and capabilities of the method

The method may be used to solve the flow on a body of revolution with any particular geometry. The local body radius and the velocity, temperature, and pressure in the potential flow outside the boundary layer should be specified. For planar flows, the invariant body radius, which is much bigger than the boundary layer width, should be specified. Two types of initial conditions, with laminar or a turbulent initial profiles, are possible. The laminar initial profiles are based on the Karman–Polhausen profile while the turbulent profiles are based on a seventh-power velocity profile. In both cases, the effects of compressibility on the initial velocity profile are neglected. The initial temperature profile depends on the initial velocity according to the Crocco integral. In both cases the initial width of the boundary layer should be determined.

4. RESULTS OF THE COMPUTATIONS

The turbulence model, numerical method and computer program described above were used to obtain solutions to various problems of transitional flow on a flat plate. The main parameters affecting transition in such a flow are the main stream Mach number, M, the main stream turbulence intensity

$$c_k = \frac{e_\infty^{1/2}}{u_\infty}$$

and the main stream length-scale Reynolds number

$$\mathrm{Re}_L = \frac{\rho_\infty u_\infty L_\infty}{\mu_\infty}$$

These parameters vary slowly in the x-direction and therefore they are prescribed at some reference point, e.g. the initial step. It should be pointed out that Re_L is not usually reported in the experimental literature while many experimental data on the influence of c_k and M on transition are available. Moreover, the present length scale L is only proportional (and not identical) to the macro-scale. Still the influence of the scale may be studied as is shown below.

4.1. Validity of the model

The present numerical scheme is based on that of Patankar and Spalding.[1] The major difference is the discarding of the wall functions. Typical results are given in Figures 3 and 4, where the variation of the transition Reynolds number and skin friction coefficient with the number of mesh points in the lateral direction N is shown, respectively. Both figures indicate satisfactory second-order convergence.

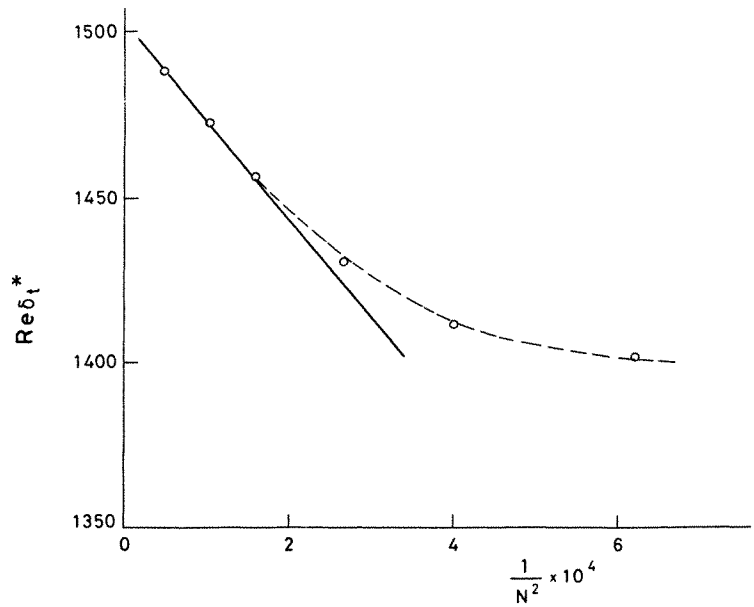

Figure 3. Variation of the transition Reynolds number in incompressible flow, on a flat plate, without pressure gradient, versus the number of mesh points

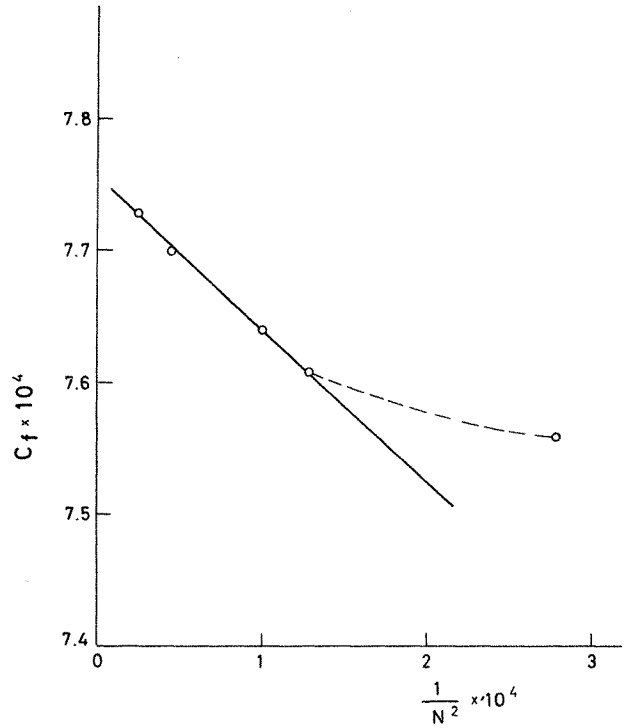

Figure 4. Variation of the friction coefficient, in incompressible flow, on a flat plate, without pressure gradient, versus the number of mesh points

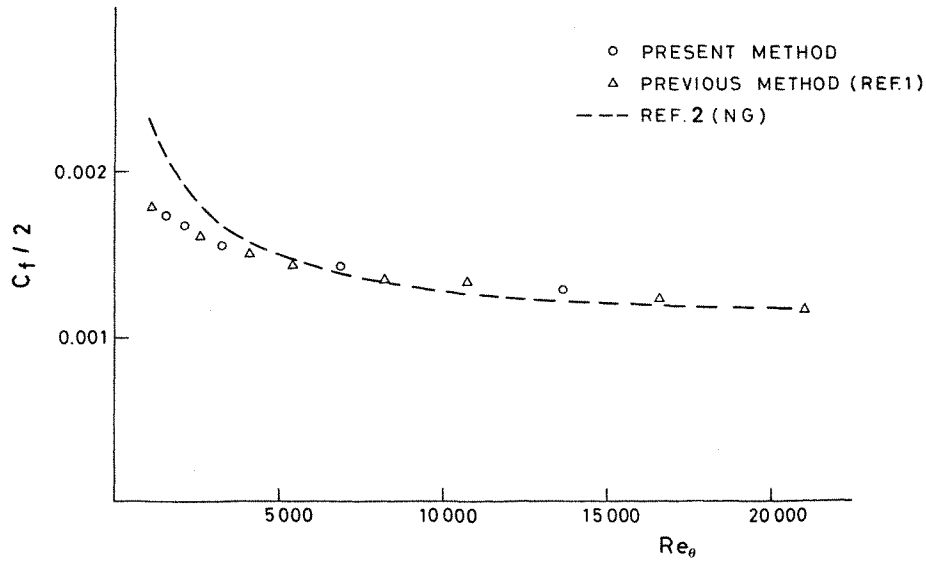

Figure 5. Friction coefficient versus momentum Reynolds number, in a turbulent incompressible flow, without pressure gradient, on a flat plate

The present turbulence model is an extension of Ng's[2] model to regions of low turbulence level. At a higher turbulence level the two models are identical. Therefore we may expect identical results in the fully turbulent region, far downstream of the transition point. Near the transition point the behaviour of the boundary layer is very sensitive to the initial and boundary conditions and therefore the present computations should differ from Ng's results in this region. This is clearly shown in Figure 5, where the skin friction coefficient, C_f, is plotted versus the momentum thickness Reynolds number, on a flat plate. The agreement with Ng's results at high Reynolds numbers suggests that the present turbulence model is as good as Ng's model, which has been compared with a large number of experimental data.

4.2. Transition calculations

For a zero pressure gradient the transition Reynolds number depends on the disturbances' amplitude and scale, and the Mach number. The disturbances' amplitude is defined as the value of turbulence energy in the potential flow e_∞. Experimental and theoretical studies show that transition from laminar to turbulent flow depends on the disturbances in the potential flow. Calculated values of the transition Reynolds number, based on displacement thickness $\left(\delta^* = \int_0^\infty \left(1 - \frac{\rho u}{\rho_\infty u_\infty}\right) dy\right)$, are plotted versus the turbulence intensity for incompressible flow in Figure 6. In these calculations the scale Reynolds number is $Re_L = 211$. The computed results are in good agreement with experimental results collected by McDonald and Fish.[17] The influence of the length scale Reynolds number, Re_L, on transition is shown in Figure 7, where the transition Reynolds number is plotted against the length scale Reynolds number for incompressible flow on a flat plate. As may be expected the transition Reynolds number decreases when Re_L increases. The effect of the Mach number on transition is shown in Figures 8 and 9. Re_{trans} rises monotonically as M increases in a parabolic way.

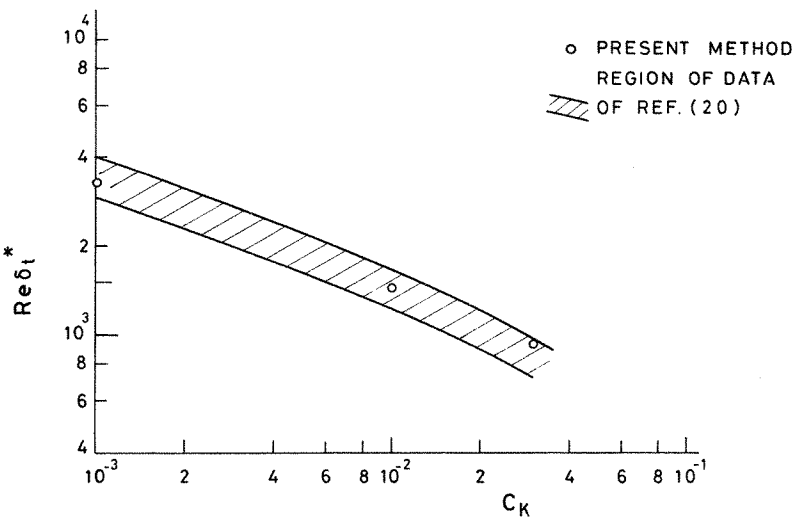

Figure 6. Comparison of calculated transition Reynolds number, in a flat plate incompressible boundary layer, with experimental data, for various main stream turbulence energy levels

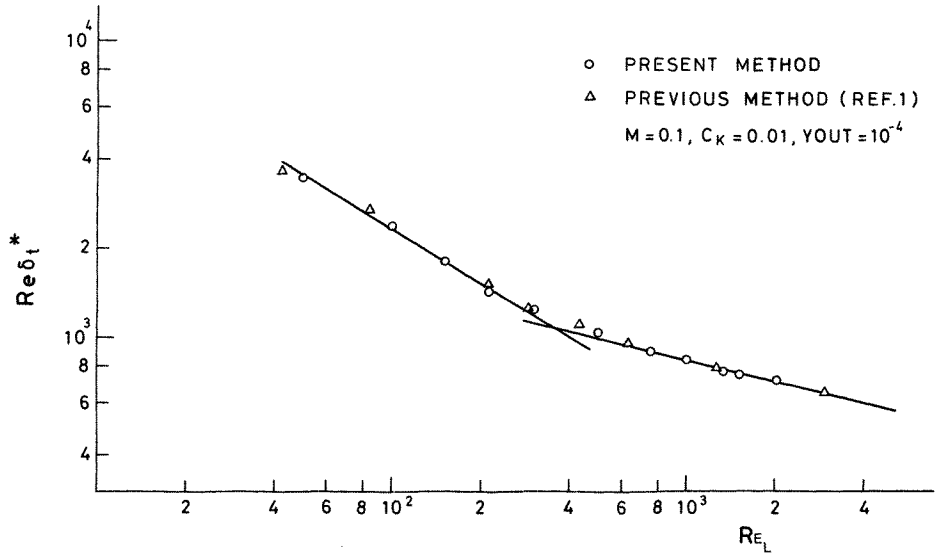

Figure 7. Transition Reynolds number, in a flat plate incompressible boundary layer versus the scale of the disturbances in the main stream

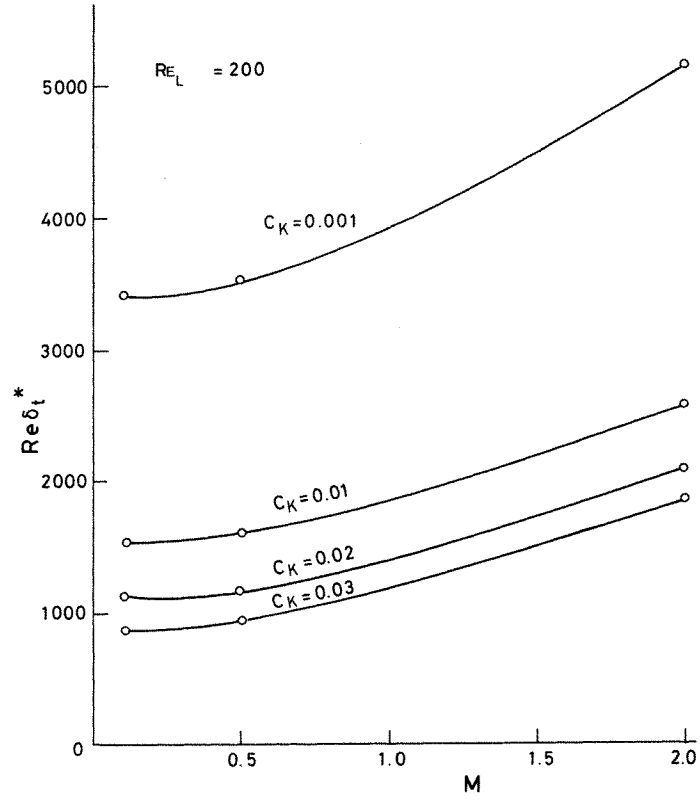

Figure 8. Transition Reynolds number versus Mach number with various turbulence energies, for $Re_L = 200$

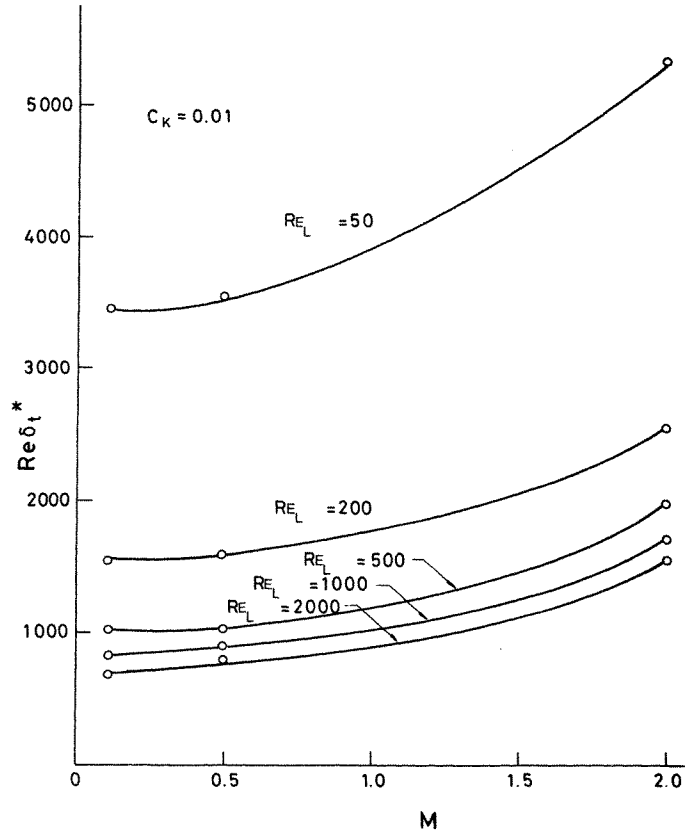

Figure 9. Transition Reynolds number versus Mach number with various length scales, for $C_k = 0{\cdot}01$

4.3. Empirical correlations

When plotting transition Reynolds number versus the turbulence intensity, length scale and Mach number, the distributions are sufficiently similar to one another to raise the possibility of finding an approximate correlation for the transition Reynolds number. Computations with combinations of Re_L varying between 50 and 2000, C_k varying between 0·001 and 0·03 and M varying between 0·1 and 2 were performed. The following correlation is in good agreement with the computations

$$Re_{\delta_t^*} = f(M)(C_k\, Re_L)^{0{\cdot}364} \tag{62}$$

with

$$f(M) = 2045 + 413M^2$$

The accuracy of the suggested formula is checked in Figure 10 where the calculated transition Reynolds number calculated by (62) is plotted against the computed $Re_{\delta_t^*}$. A very high correlation of 0·99 is achieved. Rearrangement of equation (62) is possible, when the

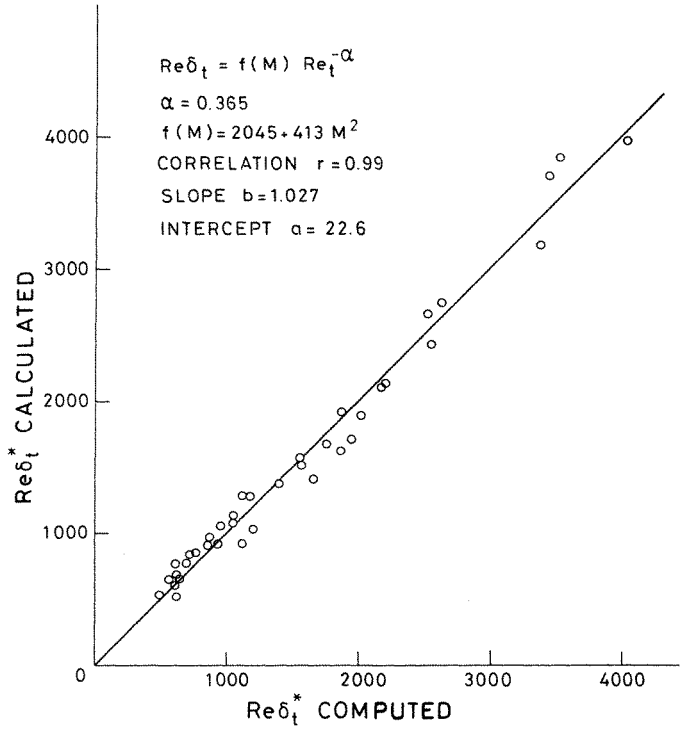

Figure 10. Comparison between computed and calculated transition Reynolds number

definitions of C_k and Re_L are recalled:

$$C_k = \frac{e_\infty^{1/2}}{u_\infty}$$

$$\mathrm{Re}_L = \frac{\rho_\infty u_\infty L_\infty}{\mu_\infty} \tag{63}$$

$$C_k\ \mathrm{Re}_L = \frac{e_\infty^{1/2}}{u_\infty}\frac{\rho_\infty u_\infty L_\infty}{\mu_\infty} = \frac{\rho_\infty e_\infty^{1/2} L_\infty}{\mu_\infty} = \mathrm{Re}_t$$

where Re_t is the turbulence Reynolds number of the main stream. Therefore

$$\mathrm{Re}_{\delta_t^*} = f(M)\ \mathrm{Re}_t^{0.364} \tag{64}$$

indicating that the transition Reynolds number depends on the free stream Mach number and the turbulence Reynolds number.

The results are subject to the following limitations:

(i) The correlations were obtained for $\mathrm{Re}_L \geq 200$.

(ii) The method of locating the transition point, identifying it as the point where the friction coefficient begins to grow is frequently inaccurate.

An improved procedure, based on the different slopes of $\log(C_f)$ versus $\log(\mathrm{Re}_{\delta_t^*})$ in laminar and turbulent flows, might improve the method, and widen the range of its effectiveness.

REFERENCES

1. S. V. Patankar and D. B. Spalding, *Heat and Mass Transfer in Boundary Layers*, 2nd edn, Int. Textbook Co. Ltd., London 1970.
2. K. H. Ng, 'Prediction of turbulent boundary-layer developments using a two equation model of turbulence', *Ph.D. Thesis*, University of London, November, 1971.
3. W. M. Kays, and E. Y. Leung, 'Heat transfer in annular passages—hydrodynamically developed turbulent flow with arbitrary prescribed heat flux', *Int. J. Heat Mass Transfer*, **6,** 537–557 (1963).
4. W. M. Kays, *Convective Heat and Mass Transfer*, McGraw-Hill, 1969.
5. E. R. van Driest, 'Investigation of laminar boundary layer in compressible fluid using the Crocco method', *NACA TN 2597* (1952).
6. R. G. Deissler, and A. L. Loeffler, 'Analysis of turbulent flow and heat transfer on a flat plate at high Mach number with variable fluid properties', *NASA TN 4262* (1958).
7. E. Reshotko, 'A program for transition research', *AIAA Paper No. 74–130* (1974).
8. M. V. Morkovin, 'Open questions-transition to turbulence at high speeds, *AFOSR TR–70–1731* (1970).
9. M. V. Morkovin, 'Critical evaluation of transition from laminar to turbulent shear layer with emphasis on hypersonically travelling bodies', *AFFDL–TR–68–149*, U.S. Air Force, March (1969).
10. E. Reshotko, 'Stability theory as a guide to the evaluation of transition data', *AIAA J.*, **7,** 1086–1091 (1968).
11. H. W. Emmons, 'The laminar–turbulent transition in a boundary layer, Pt. I'., *J. Aero. Sci.*, **7,** 490–498 (1951).
12. A. L. Nagel, 'Analysis of the unit Reynolds number effect in hypersonic flat plate boundary layer transition', *Proc. 1968 Heat Transfer and Fluid Mech. Inst.*, Seattle, June (1968), Stanford Univ. Press, pp. 51–62.
13. S. R. Pate, 'Measurement and correlations of transition Reynolds number on sharp slender cones at high speeds', *AIAA J.*, **9,** 1082–1090 (1971).
14. J. Laufer, 'Aerodynamic noise in supersonic wind tunnels', *J. Aero. Sci.*, **28,** 685–692 (1961).
15. J. E. Harris, 'Numerical solution of the equations for compressible laminar, transitional and turbulent boundary layers and comparison with experimental data', *NASA TR–R–368* (1971).
16. S. J. Shamroth, and H. McDonald, 'Assessment of a transitional boundary layer theory at low supersonic Mach numbers', *NACA CR–2131*, Nov. (1972).
17. H. McDonald, and R. W. Fish, 'Practical calculation of transitional boundary layers', *Int. J. Heat and Mass Transfer*, **16,** 1729–1974 (1973).
18. C. du P. Donaldson, 'A computer study of an analytical model of boundary-layer transition', *AIAA J.*, **2,** 271–278 (1969).
19. M. Wolfshtein, 'On the length-scale-of-turbulence equation', *Israel J. Technology*, **8,** 1–2, 87–99 (1970).
20. J. C. Rotta, 'Ueber eine methode zur berechnung turbulence scherstromungsfelder', Aerodynamische Versuch-sanstalt, Gottingen, *Report No. 69A14.*
21. W. P. Jones, and B. E. Launder, 'The prediction of laminarisation with a two equation model of turbulence', *Int. J. Heat and Mass Transfer*, **15,** 301–314 (1972).
22. F. H. Harlow, and P. I. Nakayama, 'The transport of turbulence energy decay rate', *Los Alamos Scientific Lab. Rep. LA 3854* (1968).
23. G. S. Glushko, 'Turbulent boundary layer on a flat plate in an incompressible fluid', *Izv. Akad. Nauk, SSSR*, Mekh. No. 4, pp. 13–23 (1965).
24. P. G. Saffman, 'A model for inhomogeneous turbulent flow'. *Proc. Roy. Soc., Lond.*, **A317,** 417–433 (1970).
25. D. C. Wilcox, and I. E. Alber, 'A turbulence model for high speed flows', *23rd Heat Transfer and Fluid Mechanics Inst., Proc.*, North Ridge, Cal., June (1972).
26. M. Wolfshtein, D. Naot, and A. Lin, 'Models of turbulence', in *Topics in Transport Phenomena* (Ed. C. Gutfinger), Hemisphere, 1975.
27. M. Berger, M. Israeli, and M. Wolfshtein, 'Numerical solution of transitional boundary layers', *Proc. IMACS Cong.*, Sorrento (1979).